APPLIED RESEARCH

A Novel System for Ocular Surface Temperature Measurement and Tracking

EHSAN ZARE BIDAKI[1,2]**, ALEXANDER WONG**[1]**, (Senior Member, IEEE), AND PAUL J. MURPHY**[2]
[1]Department of Systems Design Engineering, University of Waterloo, Waterloo, ON N2L 3G1, Canada
[2]School of Optometry and Vision Science, University of Waterloo, Waterloo, ON N2L 3G1, Canada

Corresponding author: Ehsan Zare Bidaki (ehsanzb@uwaterloo.ca)

ABSTRACT Ocular surface temperature (OST) is affected by changes in eye physiology caused by normal homeostasis, environmental changes, or systemic and local disease. OST can help a physician diagnose eye disease with improved accuracy and provide useful information for eye research. This paper presents a novel system, including novel hardware design and novel algorithms, capable of automatically measuring and tracking OST from the cornea over any period of time. The system uses an infrared (IR) camera and a visible (VIS) camera to capture synchronous thermal and visible videos, respectively, from the eye surface. The frames for each camera video sequence are then registered together (video registration) using two sets of control points. The points are manually selected on the first pair of timestamped IR/VIS frames and tracked over all subsequent frames using the Lucas–Kanade (LK) optical flow algorithm (point tracking). A mean square error (MSE) of 5.43±2.01 pixels was reported for salient point tracking of the IR video and 6.81±2.32 pixels for tracking of the VIS video. Overall MSE for registration was 5.03 ±1.82 pixels. The corneal area was segmented in the VIS images and localized on the IR images using the semantic segmentation method (corneal segmentation). A mean Intersection over Union (IoU) of 94.6% was found, representing the accuracy of corneal segmentation. A system for measuring and tracking eye surface temperature over time was developed. The system is able to localize the cornea on both VIS and IR images, and report temperature profiles of the cornea over the period of measurement. Experimental results show that the system can work as a tool for measuring and tracking OST over time.

INDEX TERMS Dual camera imaging system, eye temperature, ocular semantic segmentation, ocular surface temperature, thermal imaging.

I. INTRODUCTION

Human body temperature is a health biomarker. Temperature measurement is used to investigate physiological and pathological changes in the human body. For example, a raised body temperature could be a sign of infection or inflammation. Different methods are used to measure body temperature [1]. Among these methods, thermography is attractive because it is non-invasive (no temperature alteration), fast, and can show temperature distribution over the measurement area [2], [3]. Infrared (IR) thermography has been used as a non-invasive method of ocular surface temperature measurement to assist clinicians in diagnosing

The associate editor coordinating the review of this manuscript and approving it for publication was Junhua Li.

ocular disease [4], [5], [6], [7], [8], [9], [10], [11], [12], [13], [14], [15], [16], [17]. IR thermography enables the examination of temperature changes of the whole cornea, or a specific area, such as the center, inferior or superior cornea [18], [19], [20], [21]. Mapstone was the first to measure OST by a non-contact method using a bolometer (thermal detector) to measure the IR radiation from the surface of the eye [22]. In the 1970s, new cameras with improved IR sensitivity and magnification (field of view) provided an improved facility to capture OST, but were hindered by their size and the need to use liquid nitrogen [20].

Currently, there is no commercial device to measure and track temperature distribution over the eye surface in the clinical situation. Instead, researchers are using available thermal cameras which have limited analysis tools.

Published studies reporting on the measurement of OST describe varying methods for analysis of the captured IR thermography image [23]. The methods for estimation of the OST can be grouped into two categories: single camera and dual camera systems that use three methods: manual, semi-automatic, and automatic.

A single camera system only uses an IR camera, but localization of the cornea as the region of interest (ROI) is limited due to the lack of thermal distinction across the ocular surface. Dual camera systems use a visible (VIS) camera in combination with the IR camera to assist in locating specific ROI on the ocular surface. However, current systems do not synchronize these two video streams and are unable to accurately locate and track the corneal area in the IR frames during a measurement sequence. This limits the options for tracking changes in temperature over time, as well as limiting the possible analysis of OST across the cornea during the measurement period.

In a manual method, the user selects a single point, multiple points, or an area in the ROI from which an average OST is measured [18], [19], [24], [25], [26]. Manual methods, while simple in their performance, have deficiencies due to the camera technology – e.g., low thermal resolution and temporal accuracy, varying degrees of invasiveness – or from the limitations in data analysis – e.g., they are non-automatic and require much image post-processing. Researchers have attempted to improve the measurement by improving the IR camera capabilities and by implementing image processing algorithms [27], [28], [29], [30].

Another approach is based on a dual camera system that uses the VIS image to identify the ROI in the IR image, and so improve the accuracy of the segmentation [31], [32], [33], [34]. However, adjusting two cameras to have the same field of view (FOV) is difficult, and the resultant images from the two different sources are not identical in size. Furthermore, images from different sensors can be affected by many factors, such as pixel size, image resolution, lens distortion, environment light, distance, angle of photography, and sensor type. Therefore, working only on camera installation alignment will not yield data extraction with a high spatial accuracy. Previous systems were also unable to detect and remove artefacts in the OST data due to eye movement and eyelid closure. Lastly, they are not fully automatic. Therefore, an improved system is required to measure and track temperature profile reliably over time.

There are challenges in developing such a system, including: 1. Choice of suitable IR and VIS cameras able to capture appropriate details of the eye surface; 2. Design camera mounts to meet system requirements; 3. Synchronize the two cameras to capture synchronous video files of the eye surface; 4. Overlay the two video files of the eye surface such that they have the same coordinates for the corneal area on corresponding frames; 5. Localise the cornea automatically on both IR and VIS video files; 6. Detect and remove artefacts from the video files; 7. Extract and analyse temperature profile from the IR video. This paper reports on the development of a system for addressing these challenges.

II. MATERIALS AND METHODS

The system design depends on two development stages: hardware design and algorithm development. Figure 1 shows the whole system design and development process.
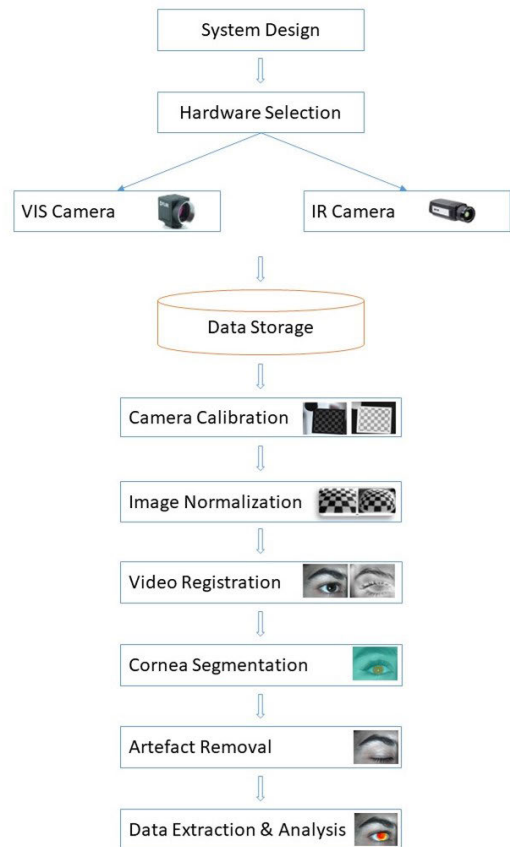

FIGURE 1. System diagram showing the different system design and development steps.

A. SYSTEM DESIGN AND HARDWARE SELECTION (CHALLENGES 1 AND 2)

A dual camera system consisting of an IR camera and a VIS camera is optimal for measuring and tracking OST over time. A Teledyne FLIR IR A655sc IR (thermal) camera (Teledyne FLIR LLC, Wilsonville, OR, USA) with geranium close-up lens was chosen to record detailed temperature information from the eye surface. A FLIR BFS 51S5C-C machine vision camera (Teledyne FLIR LLC, Wilsonville, OR, USA) with Fujinon HF12.5SA-1 close-up lens (Fujifilm Corp, Tokyo, Japan) was selected for the VIS camera. The cameras were installed on a slit-lamp biomicroscope arm with a custom-designed camera mount. The camera mount was designed to allow installation of the cameras side-by-side in front of the subject eye with minimum differential angle of photography. The mount was adjustable to change relative position of

the cameras. With this arrangement, video capture of the eye surface was possible at different observation angles and height. Figure 2 shows the camera mount and the whole system.

FIGURE 2. Mounting arrangement for the system, showing the dual camera mounting on the slit-lamp biomicroscope arm, and camera alignment with the subject headrest.

The VIS camera Horizontal FOV (38°) was adjusted to match the IR camera Horizontal FOV (5°). The same image size (640 × 480 pixels) was chosen for both cameras. The frame rate was set to 25 fps for both cameras (a frame is captured every 40ms). Camera shutter synchronization was aligned via a hardware trigger using the IR camera as primary. Video recording by the system produced two synchronous video files that were ready for processing.

B. ALGORITHM DESIGN AND DEVELOPMENT (CHALLENGES 3 – 7)
To record and process the acquired IR and VIS video files, a series of algorithms was developed.

1) VIS/IR CAMERA MANAGEMENT ALGORITHM
An algorithm was developed to manage the cameras and acquire synchronous frames from both cameras with frame timestamps. The developed algorithm was able to record individual image sequences from each camera synchronously. Figure 3 shows the developed software output for the synchronous video recording. Alignment of synchronization was determined by comparing frame timestamps and by visual comparison of side-by-side IR and VIS video frames.
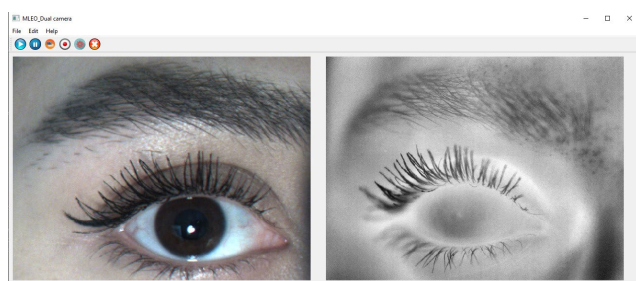

FIGURE 3. Graphical user interface (GUI) for the dual camera management software showing the software control buttons (top left), VIS camera feed (left) and IR camera feed (right).

2) VIS/IR IMAGE NORMALIZATION
An image captured by a camera will be affected by the quality of the camera lens optics and the sensor array regularity. Image distortion was considered the most important aberration. To correct for these errors in the image sequences recorded by each camera, the images were pre-processed to remove the inherent aberrations of each camera in a step called image normalization in this paper. Several images of a checkerboard pattern were required to calibrate each camera (Figure 4). A checkerboard printed on card was not suitable as it did not produce a strong IR camera image. St-Laurent et al. [35] demonstrated that aluminium is the best foundation material since it possesses a low emissivity. Based on this data, a checkerboard design was produced on a sand-blasted piece of aluminium. Since the maximum possible focus distance for the IR camera was 17 cm with a 5° FOV, the checkerboard pattern was printed on a small (8 × 6 cm) plate.
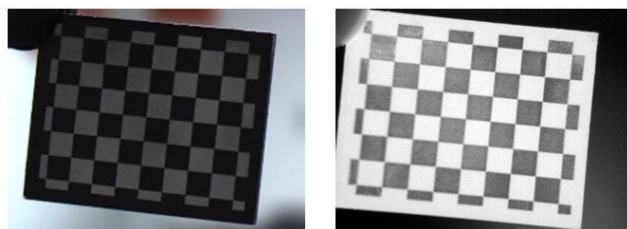

FIGURE 4. Image normalization target using a checkerboard pattern printed on a sand-blasted aluminium sheet; VIS camera (left), IR camera (right).

Using a captured single image for each camera, the camera parameters were calculated and used to calibrate the cameras. The re-projection errors were calculated as 0.38 mm and 0.52 mm for the VIS and IR cameras, respectively. The calculated parameters remain unchanged for future recording and were used to remove distortion from the recorded video frames.

3) VIS/IR VIDEO REGISTRATION
In a later step of system development, the VIS image was used to localize the cornea, by using the VIS corneal localization to identify the corneal area in the IR image. After normalizing the video files from each camera, each pixel on each VIS video frame had a matching pixel in the corresponding IR video frame. However, because of the misalignment of the two cameras, there were translational and rotational errors between the two images. Therefore, the video files were registered to ensure each corresponding pixel had the same coordinates in all subsequent VIS and IR videos. For video registration, corresponding frames in each camera vide sequence were mapped with each other. To do so, a set of corresponding control points (CPs) was selected on a pair of corresponding frames at the start of the two video sequences. The first set of CPs were manually selected on the first VIS and IR frames. Then, the points were automatically localized on all subsequent frames using the Lucas and Kanade (LK)

VIS video	MSE ± SD = 4.67 ±1.25 pixels
IR video	MSE ± SD = 5.11 ±1.79 pixels

TABLE 2. Mean IOU output from the four tested segmentation models.

Model	Mean IoU (%)
FCN32	89.2
SegNet	92.3
UNet	91.7
PSPNet	94.6

[36] optical flow algorithm, and the corresponding CPs on each set of corresponding frames were registered using Affine transformation. To check system accuracy, six synchronous video files (VIS/IR) were recorded from the eye surface. The cameras were set to 25 fps to record a total number of 250 frames for each video over 10 seconds. After the pre-processing step, the first images of each video file were shown side-by-side to select the corresponding CPs on the first frames and the points were localized on all video frames using the LK optical flow algorithm. Table 1 shows the calculated error for point localization of the video files.

After localizing the control points in each frame, the video files were registered using the point coordinates of the control points on the visible and thermal frames, using the Affine image registration algorithm [37]. Any misplacement of the points in the registration process is known as the fiducial registration error. The mean fiducial registration error (FRE) for all of video files was 4.79 ± 1.22 (SD) pixels.

4) VIS CORNEA LOCALIZATION
A key system aim was to extract OST values for the cornea from each IR video frame. However, IR image formation is based on the temperature distribution across the ocular surface and there was no clear boundary that separated the cornea from the conjunctiva in the IR images. Video registration of the dual camera system produced an aligned VIS and IR image. The cornea was localized in the IR image by using the VIS image to identify and segment the cornea, and then using the segmented area in the VIS image as a mask over the IR image to locate the cornea. The limits of the cornea on the VIS image were found by identifying the underlying colored iris, since the outer boundary of iris provided a strong contrasting signal to the neighboring white sclera. Semantic segmentation was used in to segment the cornea from the VIS image (Figure 5). Four different networks (FCN32, SegNet, U-Net, and PSPNet) were trained and the accuracy of each network compared to choose the best semantic segmentation method. PSPNet was found to give the highest accuracy for cornea segmentation using Mean Intersection of Union (IOU) (Table 2).

5) VIS IMAGE SEGMENTATION ONTO IR IMAGE
Figure 6 shows a sequence of mapped video frames after the full algorithm implementation. The figure shows extracted
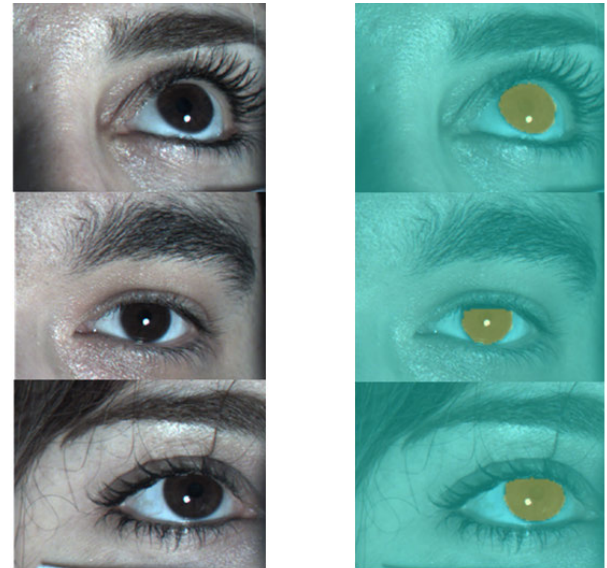

FIGURE 5. Cornea segmentation results of 3 sample images from the video image database; VIS image (left), VIS image with segmentation mask (right). The yellow areas show the cornea pixels detected by the network.

consecutive frames from the video file between two blinks. The segmented corneal ROI from the thermal image has been mapped onto the corneal area of the visible image. The different colors in the thermal images represent different temperatures across the corneal ROI.

6) VIS BLINK AND EYE MOVEMENT ARTEFACT REMOVAL
When analyzing the VIS video files, artifacts were observed due to the presence of a blink or eye movement within a frame. To remove these artifacts, the segmentation network was used as a blink detection tool. When the iris segmentation network failed to detect a cornea in the image, the network could distinguish between blink and non-blink frames and remove frames containing a blink from the analysis step (Figure 7). To assess the blink detection algorithm accuracy, the blink detection output was compared with a manual review of six IR video files (250 frames) for presence of blink in the image. The number of incorrectly identified frames by the blink detection algorithm were noted and compared to the number of frames detected manually. An accuracy of 99.4% was determined for algorithm blink detection. A second artefact, associated with eye movement, was also addressed by using the corneal segmentation algorithm in the VIS video sequence. When the cornea was localized in each VIS frame of the sequence, the cornea segmentation network predicted the detected corneal area from the produced segmentation masks. Frames in which corneal segmentation was <30% were removed from the analysis. In this way, the corneal area was tracked in both the visible and thermal video files ensuring that surface temperature was only extracted from the cornea ROI for further analysis.
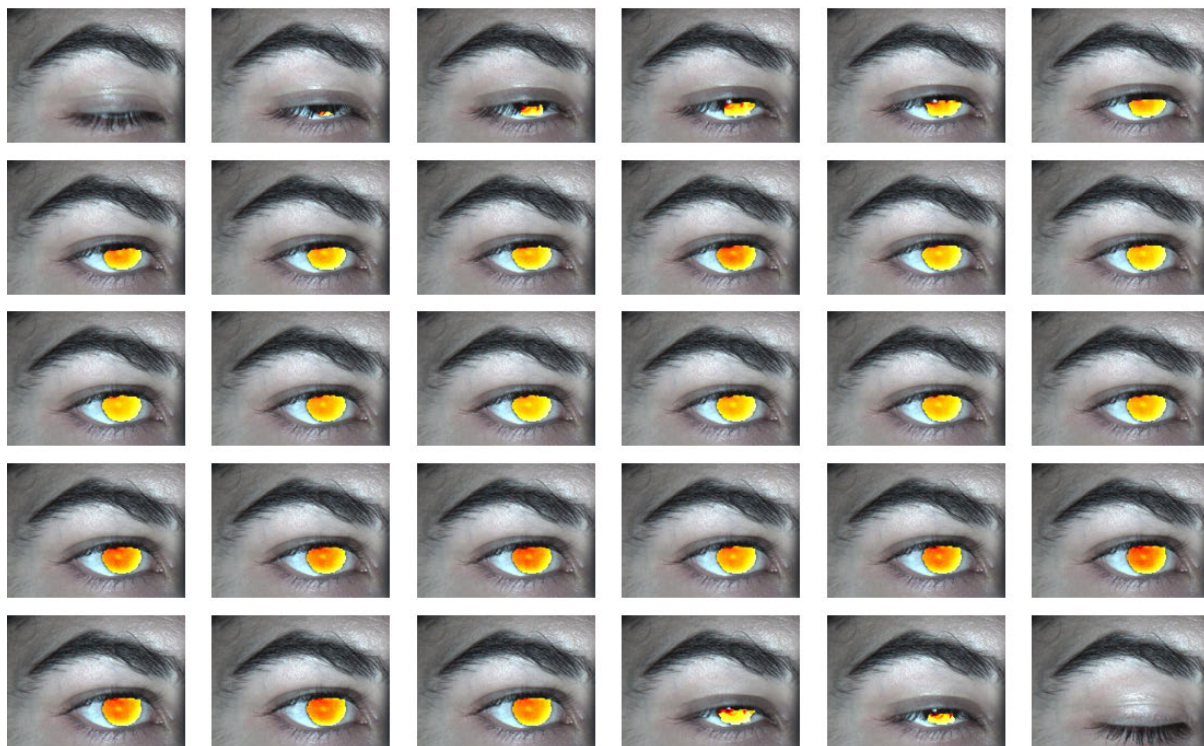
FIGURE 6. Sample frames from a VIS video sequence delimited by two blinks showing mapping of the segmented IR corneal ROI onto the VIS image. Where no IR image is mapped, no cornea was detected in the VIS frame due to blinking.

FIGURE 7. Predicted masks by the network showing IR video frames in which the subject had blinked.
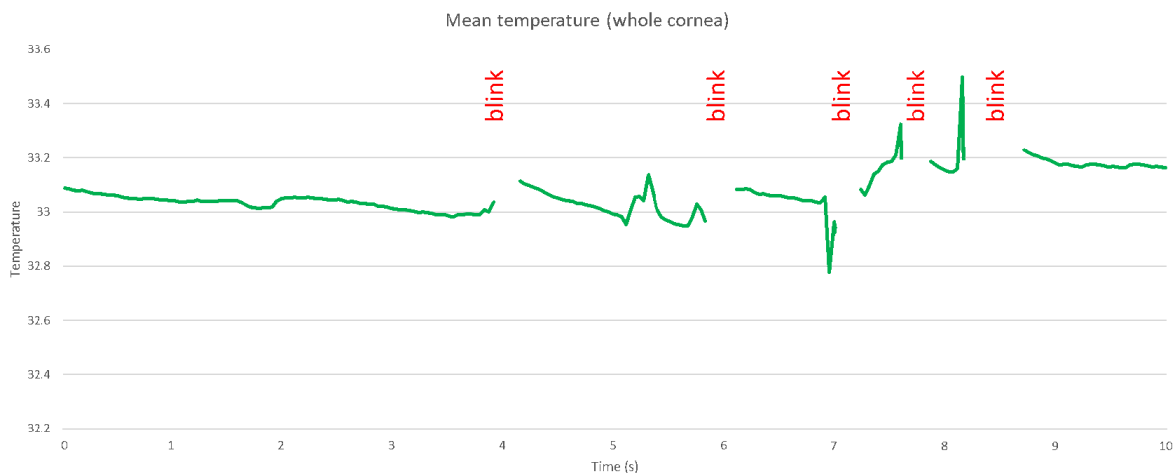

FIGURE 8. Average temperature (°C) tracking for the whole corneal ROI over a 10 second period. Recording began immediately after a blink. Gaps in trace represent non-analyzed frames that were removed due to presence of a blink.

7) TEMPERATURE EXTRACTION

The system was able to extract the temperature profile of the cornea ROI from the eye surface for further analysis. Figure 8 shows a sample temperature change trace (°C) produced for the average temperature tracked over the whole cornea ROI. Analysis can be made for whole cornea, corneal center,

superior cornea, inferior cornea, or any selected ROI on the eye surface.

C. DATASET

A total of 160 images of the eyes of 10 subjects were captured to produce the dataset used in this project. The images were taken of each subject's eye in a controlled illumination area with their gaze directed straight ahead, upwards, downwards, to the left, to the right, and with the eyelid closed. As the total number of images for training purpose were low, data augmentation was used in the training step. Augmentation methods used were: translation, warping, rotation, flipping, re-sizing, color-space shifting, scaling, and changing contrast.

III. CONCLUSION

OST measurement has the potential to provide useful information about ocular surface health. For example, knowledge of the OST can help a physician to diagnose some eye diseases with much improved accuracy [4], [5], [6], [7], [8], [9], [10], [11], [12], [13], [14], [15], [16], [17], [38]. It can also be used for a better understanding of tear film quality by looking at changes in OST associated with tear film break-up and associated tear evaporation [5], [10]. Current methods for assessing OST clinically are severely limited. No commercial systems for assessing OST are available and researchers have relied on customized instruments. Of the instruments available, all are designed with either one camera (IR) or two cameras (one IR and one VIS). The dual camera systems are designed to use the VIS camera to help overcome the inherent lack of spatial resolution across the IR image that makes precise identification of the corneal boundary difficult. By overlapping the FOV of both cameras, the corneal boundary in the VIS camera image can be used to locate the corneal boundary in the IR image. The lack of spatial resolution in IR cameras has also meant that researchers must rely on manual selection of individual points or ROI on the ocular surface, and to a very restricted set of options in terms of data analysis. Data analysis typically means a comparison over time between individual data points on the ocular surface or between average temperatures within selected areas on the surface across the ocular surface. When one considers that the pixel count across the cornea in the IR image typically exceeds 12000 pixels per frame of a video sequence, this simplified manual approach inevitably leads to a huge amount of detail being lost. This paper reports on the development of a novel system and method for imaging, segmenting, temporal and spatial tracking, and analysis of VIS and IR images of the ocular surface and eye adnexa. The developed system has the ability to locate the corneal area in the thermogram and consistently measure from the same location on the ocular surface by tracking and compensating for any head or eye movements. It can remove artefacts like blinking and eye movement from the recorded video files and track reliable OST changes over time. For the first time, a complete system for imaging the ocular surface,

synchronizing video sequences, segmenting the cornea, and extracting ocular surface temperature (OST) data from the eye has been developed. The calculated accuracy in each step shows that the system has the potential to be used in OST measurement and tracking.

REFERENCES

[1] C. Purslow and J. S. Wolffsohn, "Ocular surface temperature: A review," *Eye Contact Lens*, vol. 31, no. 3, pp. 117–123, 2005.

[2] R. Gade and T. B. Moeslund, "Thermal cameras and applications: A survey," *Mach. Vis. Appl.*, vol. 25, pp. 245–262, 2014.

[3] J.-H. Tan, E. Y. K. Ng, R. Acharya, and U. C. Chee, "Automated study of ocular thermal images: Comprehensive analysis of corneal health with different age group subjects and validation," *Digit. Signal Process.*, vol. 20, pp. 1579–1591, 2010.

[4] B. Chandrasekar, A. P. Rao, M. Murugesan, S. Subramanian, D. Sharath, U. Manoharan, B. Prodip, and V. Balasubramaniam, "Ocular surface temperature measurement in diabetic retinopathy," *Experim. Eye Res.*, vol. 211, Oct. 2021, Art. no. 108749.

[5] A. M. Shah and A. Galor, "Impact of ocular surface temperature on tear characteristics: Current insights," *Clin. Optometry*, vol. 13, pp. 51–62, Feb. 2021.

[6] S. Matteoli, E. Favuzza, L. Mazzantini, P. Aragona, S. Cappelli, A. Corvi, and R. Mencucci, "Ocular surface temperature in patients with evaporative and aqueous-deficient dry eyes: A thermographic approach," *Physiol. Meas.*, vol. 38, no. 8, pp. 1503–1512, Jul. 2017.

[7] M. Rolando and M. Zierhut, "The ocular surface and tear film and their dysfunction in dry eye disease," *Surv. Ophthalmol.*, vol. 45, pp. S203–S210, Mar. 2001.

[8] H. Naidorf-Rosenblatt, D. Landau-Part, J. Moisseiev, A. Alhalel, R. Huna-Baron, A. Skaat, S. Pilus, L. Levi, and A. Leshno, "Ocular surface temperature differences in retinal vascular diseases," *Retina*, vol. 42, no. 1, pp. 152–158, 2022.

[9] T. Rosenstock, P. Chart, and J. J. Hurwitz, "Inflammation of the lacrimal drainage system–assessment by thermography," *Ophthalmic Surg.*, vol. 14, no. 3, pp. 229–237, Mar. 1983.

[10] P. B. Morgan, A. B. Tullo, and N. Efron, "Ocular surface cooling in dry eye—A pilot study," *J. Brit. Contact Lens Assoc.*, vol. 19, no. 1, pp. 7–10, 1996.

[11] P. B. Morgan, J. V. Smyth, A. B. Tullo, and N. Efron, "Ocular temperature in carotid artery stenosis," *Optometry Vis. Sci.*, vol. 76, no. 12, pp. 850–854, Dec. 1999.

[12] S. Tokuoka, M. Nakajima, J. Nishikawa, H. Kuroda, and I. Azuma, "Cold response of skin and eye temperature in glaucoma," *Folia Ophthalmol. Japan*, vol. 41, pp. 1159–1165, 1990.

[13] P. Bourjat and M. Gautherie, "Unilateral exophthalmos investigated by infrared thermography," *Mod. Problems Ophthalmol.*, vol. 14, pp. 278–285, Jan. 1975.

[14] J. Hannerz, "Pain characteristics of painful ophthalmoplegia (the Tolosahunt Syndrome)," *Cephalalgia*, vol. 5, no. 2, pp. 103–106, Jun. 1985.

[15] G. Cardona, P. B. Morgan, N. Efron, and A. B. Tullo, "Ocular and skin temperature in ophthalmic postherapeutic neuralgia," *The Pain Clinic*, vol. 9, no. 2, pp. 145–150, 1996.

[16] B. IuB, O. P. Lenskaia, and B. M. Belkina, "Thermography in the diagnosis of retinoblastoma in children," *Meditsinskaia Radiologiia*, vol. 30, no. 12, pp. 19–21, 1985.

[17] A. I. Eremenko, "Thermography in the diagnosis of vascular neuritis of the optic nerve," *Oftalmologicheskii Zhurnal*, vol. 4, pp. 235–239, Dec. 1985.

[18] P. J. Murphy, P. B. Morgan, S. Patel, and J. Marshall, "Corneal surface temperature change as the mode of stimulation of the non-contact corneal aesthesiometer," *Cornea*, vol. 18, no. 3, pp. 333–342, May 1999.

[19] N. Efron, G. Young, and N. A. Brennan, "Ocular surface temperature," *Curr. Eye Res.*, vol. 8, no. 9, pp. 901–906, 1989.

[20] R. Mapstone, "Ocular thermography," *Brit. J. Ophthalmol.*, vol. 54, no. 11, p. 751, 1970.

[21] A. R. Fielder, A. F. Winder, G. A. Sheraidah, and E. D. Cooke, "Problems with corneal arcus," *Trans. Ophthalmol. Soc. U.K.*, vol. 101, no. 1, pp. 22–26, 1981.

[22] R. Mapstone, "Determinants of corneal temperature," *Brit. J. Ophthalmol.*, vol. 52, no. 10, pp. 729–741, Oct. 1968.

[23] E. Z. Bidaki, A. Wong, and P. J. Murphy, "A novel computational thermal-visual imaging system for automatic cornea temperature measurement and tracking," *J. Comp. Vis. Imag. Syst.*, vol. 8, no. 1, pp. 20–23, 2022.

[24] P. B. Morgan, A. B. Tullo, and N. Efron, "Infrared thermography of the tear film in dry eye," *Eye*, vol. 9, no. 5, pp. 615–618, Sep. 1995.

[25] H. K. Chiang, C. Y. Chen, H. Y. Cheng, K.-H. Chen, and D. O. Chang, "Development of infrared thermal imager for dry eye diagnosis," *Proc. SPIE*, vol. 6294, pp. 36–43, Sep. 2006.

[26] E. Y. K. Ng, J. H. Tan, E. H. Ooi, C. Chee, and U. R. Acharya, "Variations of ocular surface temperature with different age groups," in *Image Modeling of Human Eye*. Norwood, MA, USA: Artech House, 2008.

[27] R. A. U, E. Y. K. Ng, G. C. Yee, T. J. Hua, and M. Kagathi, "Analysis of normal human eye with different age groups using infrared images," *J. Med. Syst.*, vol. 33, no. 3, pp. 207–213, Jun. 2009.

[28] S. Matteoli, D. Coppini, and A. Corvi, "A novel image processing procedure for thermographic image analysis," *Med. Biol. Eng. Comput.*, vol. 56, no. 10, pp. 1747–1756, Oct. 2018.

[29] J.-H. Tan, E. Y. K. Ng, and R. A. U, "Automated detection of eye and cornea on infrared thermogram using snake and target tracing function coupled with genetic algorithm," *Quant. Infr. Thermography J.*, vol. 6, no. 1, pp. 21–36, Jun. 2009.

[30] S. Zheng, D. Fu, T. Yang, L. Luo, and X. Nan, "A novel method for eye contour extraction from blurred infrared images," in *Proc. 8th Int. Conf. Intell. Hum.-Mach. Syst. Cybern. (IHMSC)*, vol. 1, Aug. 2016, pp. 103–106.

[31] T. Kamao, M. Yamaguchi, S. Kawasaki, S. Mizoue, A. Shiraishi, and Y. Ohashi, "Screening for dry eye with newly developed ocular surface thermographer," *Amer. J. Ophthalmol.*, vol. 151, no. 5, pp. 782–791.e1, May 2011.

[32] T.-Y. Su, S.-W. Chang, C.-J. Yang, and H. K. Chiang, "Direct observation and validation of fluorescein tear film break-up patterns by using a dual thermal-fluorescent imaging system," *Biomed. Opt. Exp.*, vol. 5, no. 8, pp. 2614–2619, 2014.

[33] W. Li, A. D. Graham, S. Selvin, and M. C. Lin, "Ocular surface cooling corresponds to tear film thinning and breakup," *Optometry Vis. Sci.*, vol. 92, no. 9, pp. e248–e256, 2015.

[34] H. Kricancic, H. McNeill, M. Titze, D. Alonso-Caneiro, and M. J. Collins, "Instrument for simultaneous assessment of fluorescein and thermal dynamics of the tear film," in *Proc. ARVO ASIA Meeting*, 2017. [Online]. Available: https://eprints.qut.edu.au/105600/

[35] L. St-Laurent, M. Mikhnevich, A. Bubel, and D. Prévost, "Passive calibration board for alignment of VIS-NIR, SWIR and LWIR images," *Quant. Infr. Thermogr. J.*, vol. 14, no. 2, pp. 193–205, Jul. 2017.

[36] B. D. Lucas and T. Kanade, "An iterative image registration technique with an application to stereo vision," in *Proc. 7th Int. Joint Conf. Artif. Intell.*, vol. 81, Vancouver, BC, Canada, Aug. 1981, pp 674–679.

[37] R. Hartley and A. Zisserman, *Multiple View Geometry in Computer Vision*. Cambridge, U.K.: Cambridge Univ. Press, 2003.

[38] M. A. Lemp and G. N. Foulks, "The definition and classification of dry eye disease," *Ocul. Surf.*, vol. 5, no. 2, pp. 75–92, 2007.
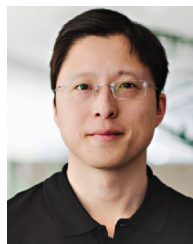
ALEXANDER WONG (Senior Member, IEEE) received the B.A.Sc. degree in computer engineering, the M.A.Sc. degree in electrical and computer engineering, and the Ph.D. degree in systems design engineering from the University of Waterloo, Waterloo, ON, Canada, in 2005, 2007, and 2010, respectively. He is currently the Canada Research Chair of artificial intelligence and medical imaging, the Co-Director of the Vision and Image Processing Research Group, and a Professor with the Department of Systems Design Engineering, University of Waterloo. He is a fellow of the Royal Society of Public Health, Institution of Engineering and Technology, Institute of Physics, and International Society for Design and Development in Education. He has authored over 600 refereed journals and conference papers and patents, in various fields, such as computational imaging, artificial intelligence, computer vision, graphics, image processing, and multimedia systems. His research interests include integrative biomedical imaging systems design, operational artificial intelligence, and scalable and explainable deep learning. He is a member of the College of the Royal Society of Canada. He has received a number of awards, including two outstanding performance awards, the Distinguished Performance Award, the Engineering Research Excellence Award, the Sandford Fleming Teaching Excellence Award, the Early Researcher Award from the Ministry of Economic Development and Innovation, two magna cum laude awards and the Cum Laude Award from the Annual Meeting of the Imaging Network of Ontario, the Alumni Gold Medal, the Outstanding Paper Award at the IEEE/CVF Conference on Computer Vision and Pattern Recognition (CVPR) Workshop on Adversarial Machine Learning in Real-World Computer Vision Systems and Online Challenges, in 2021, the Best Paper Award at the Conference on Neural Information Processing Systems (NIPS) Workshop on Transparent and Interpretable Machine Learning, in 2017, the AquaHacking Challenge First Prize, in 2017, the Best Student Paper at the Ottawa Hockey Analytics Conference, in 2017, the Best Paper Award at the NIPS Workshop on Efficient Methods for Deep Neural Networks, in 2016, the Synaptive Best Medical Imaging Paper Award, in 2016, the Distinguished Paper Award by the Society of Information Display, in 2015, the Best Paper Award at the Conference of Computer Vision and Imaging Systems, in 2015 and 2017, and the Best Paper Award by the Canadian Image Processing and Pattern Recognition Society, in 2009 and 2014.

EHSAN ZARE BIDAKI received the B.Sc. and M.Sc. degrees in computer engineering (image processing) from Science and Research University, Tehran, Iran, in 2006 and 2010, respectively, the joint Graduate degree from the Optometry School and System Design Engineering Departments, University of Waterloo, and the Ph.D. degree, in 2022, under supervision of Prof. Paul Murphy and Prof. Alexander Wong. His Ph.D. dissertation was titled "A System for Ocular Surface Temperature Measurement and Tracking Using Infrared Thermography." He was a Lecturer with Islamic Azad University, Tehran, from 2010 to 2016. Currently, he is a PDF in the Department of Systems Design Engineering and the School of Optometry and Vision Science, University of Waterloo, investigating a novel system for ocular surface temperature measurement and tracking under supervision of Prof. Paul Murphy and Prof. Alexander Wong. His research interests include ocular surface image analysis, ocular surface temperature measurement, machine vision, machine learning, and thermal image analysis.

PAUL J. MURPHY received the B.Sc. degree from Cardiff University, in 1988, the Ph.D. degree from Glasgow Caledonian University, in 1996, and the M.B.A. degree from the University of South Wales, in 2013. Previously, he was an Assistant Professor with Glasgow Caledonian University and an Associate Professor with Cardiff University. He is currently a Full Professor with the University of Waterloo, Canada. His primary research interests include optometric instrumentation design, thermography, evaporimetry, and anterior eye physiology. He is a fellow of the College of Optometrists, U.K., American Academy of Optometry, European Academy of Optometry and Optics, and the British Contact Lens Association.

● ● ●